International Journal of Mass Spectrometry 280 (2009) 154–161

Contents lists available at ScienceDirect

International Journal of Mass Spectrometry

journal homepage: www.elsevier.com/locate/ijms

Singlet and triplet state dynamics of charge and hydride transfer reactions of OD^+ ($\mathbf{X}^3\Sigma^-$) with propyne

Li Liu, Yue Li[1], James M. Farrar*

Department of Chemistry, University of Rochester, Rochester, NY 14627, United States

ARTICLE INFO

Article history:
Received 13 June 2008
Received in revised form 1 August 2008
Accepted 6 August 2008
Available online 15 August 2008

Keywords:
Ion–molecule reactions
Charge transfer
Hydride transfer
Potential energy surfaces
Intersystem crossing

ABSTRACT

We report a crossed beam study of the title reactions in the collision energy range from 0.45 to 1.23 eV (43–119 kJ/mol). Both reactions are exoergic and proceed as direct processes on a time scale much less than the rotational period of the transient association complex of approaching reactants. The charge transfer process takes place with zero momentum transfer. Density Functional Theory calculations of the structures of reactive intermediates show that a plausible pathway for hydride transfer involves initial charge transfer on a triplet surface, followed by intersystem crossing to the singlet manifold. This process is followed by rapid hydrogen atom transfer to form an intermediate that dissociates smoothly to products. The kinematics of the heavy + light-heavy mass combination result in mixed energy release at the lowest collision energy, in which both the breaking and forming bonds are extended, while at higher collision energies, the incremental translational energy in the reactants appears preferentially in product translation, consistent with induced repulsive energy release.

1. Introduction

The reactivity of ground state (^{3}P) oxygen atoms with unsaturated hydrocarbons is a topic that has received significant experimental and theoretical attention [1–6]. The role of potential surfaces of triplet and singlet multiplicity and the structures of reactive intermediates are topics that present significant theoretical challenges important in combustion, atmospheric chemistry, and photochemistry [7,8]. Recent studies from this laboratory concerned with the isoelectronic OH^+ ($\mathbf{X}^3\Sigma^-$) species have employed ion beam methods and Density Functional Theory (DFT) calculations to probe these same experimental and theoretical issues in the reactions with ethylene [9], acetylene [10] and propylene [11] molecules. In the reactions of OH^+ with alkenes, both charge transfer and hydride transfer processes were observed. The competition between hydride transfer occurring through an oxirane diradical cation intermediate and a direct process involving sequential electron and hydrogen atom transfer was also probed as a function of the number of carbon atoms. In the OH^+ + acetylene system, hydride abstraction was not observed, although favorable; only charge transfer and proton transfer products were observed. In order to understand the different reactivities of OH^+/OD^+ ions with alkenes and alkynes, and the possible effects of methyl substitution at one of the unsaturated carbon atoms, we have examined the reactions of the isotopically labeled reactant OD^+ with propyne. In this system, charge transfer, hydride transfer, proton transfer, and charge transfer with H/D exchange were detected, summarized as follows:

$$OD^+ + C_3H_4 \rightarrow C_3H_4^+ + OD \quad \Delta H = -2.67\,eV\,(-258\,kJ/mol) \quad (1)$$

$$OD^+ + C_3H_4 \rightarrow C_3H_3^+ + HOD \quad \Delta H = -6.61\,eV\,(-638\,kJ/mol) \quad (2)$$

$$OD^+ + C_3H_4 \rightarrow C_3H_4D^+ + O \quad \Delta H = -2.72\,eV\,(-263\,kJ/mol) \quad (3)$$

$$OD^+ + C_3H_4 \rightarrow C_3H_3D^+ + OH \quad \Delta H = -2.67\,eV\,(-258\,kJ/mol) \quad (4)$$

An additional channel (5), dissociative charge transfer, is also thermodynamically possible as a route to $C_3H_3^+$.

$$OD^+ + C_3H_4 \rightarrow C_3H_3^+ + H + OD \quad \Delta H = -1.39\,eV\,(-134\,kJ/mol) \quad (5)$$

Survey mass spectra of the reaction products showed approximate branching ratios for the products $C_3H_4^+$:$C_3H_3^+$:$C_3H_4D^+$:$C_3H_3D^+$ (mass 40:mass 39:mass 42:mass 41) to be 20:10:5:1, respectively, independent of collision energy. As a function of collision energy, the relative cross sections for all products decreased by a factor of two as the collision energy increased from 0.4 to 1.2 eV. Over this range of energies, only the products $C_3H_4^+$ and $C_3H_3^+$ had sufficient

* Corresponding author. Tel.: +1 585 275 5834; fax: +1 585 276 0205.
E-mail address: farrar@chem.chem.rochester.edu (J.M. Farrar).
[1] Present address: Department of Chemistry and Biochemistry, University of Maryland, College Park, MD 20742, United States.

1387-3806/$ – see front matter © 2008 Elsevier B.V. All rights reserved.
doi:10.1016/j.ijms.2008.08.002

intensity to allow relative differential cross section measurements to be performed.

To the best of our knowledge, there is no previous detailed study of the $OH^+ + C_3H_4$ system. Prior studies of the structures and energies of several $[C_3H_5O]^+$ isomers that may serve as reaction intermediates for the present system provide guidance to this study. Bouchoux et al. investigated twelve $[C_3H_5O]^+$ structures implicated in the electron impact mass spectra of several precursor molecules with *ab initio* SCF/CI calculations using 4-31G basis sets [12]. Studies of the reactions of the isoelectronic neutral system $O(^3P) + C_3H_4$ also provide useful information for the present study. Kanofsky et al. observed products from seven reactive channels in a crossed beam experiment [13]. Blumenberg et al. concluded that reaction forming $CO + C_2H_4$ accounted for 95% of the total reaction products [14]. Arrington and Cox investigated the reactions of ground state oxygen atoms with propyne in a discharge flow system over the temperature range from 298 to 600 K and determined Arrhenius parameters for the rate constant [15]. These workers also discovered that the methyl substituent lowered the activation energy for attack of the oxygen atom on the π-electron system. Umstead et al. studied the CO products in this system by resonance absorption [16]. The observed CO vibrational populations were consistent with a statistical model predicting that the dominant initial co-product is the ethylidine radical CH_3CH, which isomerizes to C_2H_4 after the nascent products separate. Xing et al. also studied the reactions of O with several alkynes including propyne by probing the H, CO and H_2 products with vacuum ultraviolet laser-induced fluorescence [17]. The formation of singlet state products was hypothesized to occur via intersystem crossing from the initial triplet state accessed by the approaching reactants.

In this paper, we report crossed beam studies of charge transfer and hydride transfer over a relative collision energy range of 0.45–1.23 eV (43–119 kJ/mol). Calculations of possible intermediates using DFT methods provide insight into the role that triplet and singlet surfaces play in determining the reactive pathways followed by this system. In addition, the product energy disposal appears to be affected by kinematic factors associated with the heavy + light-heavy mass combination of the reactants.

2. Experimental

The experimental apparatus has been described in previous publications [18], and a recent review of the capabilities of this method has appeared in the literature [19]. OD^+ ions were produced by electron impact on deuterium oxide vapor with He gas as the carrier. The measured pressure in the initial focusing stage vacuum chamber was about 3×10^{-5} Torr, corresponding to a pressure in the ionization region of the source of $\sim 10^{-2}$ Torr. The vibrational energy distribution in the OD^+ reactants is unknown. This point is discussed in more detail in Section 3, in the context of the total energy available to reaction products. The ions were accelerated to 300 V, where mass selection was accomplished with a 60° sector momentum analysis magnet. After deceleration and focusing to the desired beam energy, the beam had a laboratory energy distribution with a FWHM of 0.30–0.45 eV. Experiments were performed at selected energies over a relative collision energy range of 0.45–1.23 eV. The propyne beam was formed by supersonic expansion of the gas (98%, Sigma–Aldrich) through a 0.07 mm nozzle. In the main chamber, the neutral beam intersected with the ion beam at 90°. A tuning fork chopper modulated the neutral beam at 30 Hz, and a multichannel scaler gated in synchronization with the beam modulation allowed background to be separated from the true reactive scattering signal. An electrostatic energy analyzer with resolution of 0.07 eV was used to measure the kinetic energy distributions of the reactant and product ions. The energy analyzer was calibrated before and after the experiments with the resonant charge transfer reaction between He^+ and He [20]. The product ions were mass-selected by a quadrupole mass spectrometer and detected by a dual microchannel plate ion detector.

Two independent measurements were performed in the experiment. At each collision energy, kinetic energy distributions of the scattered product ions were measured at 16–22 fixed laboratory angles based on the signal levels. These kinetic energy distributions were then normalized to angular distributions of product ions in the laboratory coordinate system measured by summing the signal over all energies. The angular distributions were corrected for beam drifting and detection efficiency by returning to a reference angle periodically and assuming that the drift of the signal was linear in time. These measurements were carried out at each laboratory energy.

3. Data analysis

The experimental kinetic energy and angular distributions of products were transformed to the center of mass (c.m.) coordinate system. An iterative deconvolution procedure was used to extract the c.m. cross section from the laboratory flux distributions while removing the averaging and broadening effects of the beam velocity distributions [21]. The barycentric angular distribution $g(\theta)$ and relative translational energy distribution $P(E'_T)$ of the products were calculated by appropriate integration of the derived c.m. cross section $I_{c.m.}(u,\theta)$:

$$g(\theta) = \int_0^\infty I_{c.m.}(u,\theta)\,du \tag{6}$$

$$P(E'_T) = \int_0^\pi u^{-1} I_{c.m.}(u,\theta)\,\sin\theta\,d\theta \tag{7}$$

The full flux distributions in velocity space as well as the kinetic energy and angular distributions derived from them provide important physical insight into the nature of reactive collisions.

The charge transfer reaction $OD^+ + C_3H_4 \rightarrow C_3H_4^+ + OD$ was studied at relative collision energies of 0.45, 0.71, and 1.16 eV. Fig. 1 shows the center of mass flux distribution of the $C_3H_4^+$ products at the lowest collision energy, obtained by iterative deconvolution as

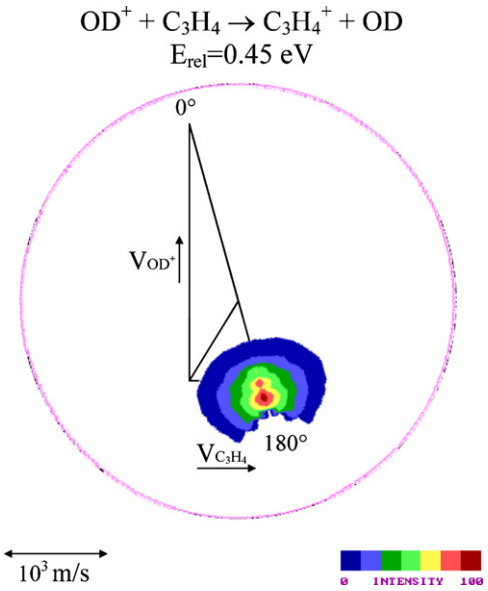

Fig. 1. Newton diagram and scattered $C_3H_4^+$ product flux contour map at the collision energy of 0.45 eV.

described previously. In the c.m. coordinate system, the directions of the OD^+ ion beam and C_3H_4 neutral beam are 0° and 180°, respectively. The flux distributions for the two higher energy experiments are qualitatively similar to Fig. 1 and are available in Supplementary Information for this paper.

The experimental results shown in the velocity space map indicate that the charge transfer flux distribution is sharply asymmetric. The majority of the $C_3H_4^+$ products are scattered in the same direction as the precursor C_3H_4 beam with similar velocities. These forward-scattered products indicate that the charge transfer reaction is dominated by a direct mechanism, proceeding through large impact parameter collisions on a time scale much shorter than a rotational period of the transient association complex of the approaching reactants.

The angular distributions and relative translational energy distributions of the charge transfer products at all three energies are shown in Fig. 2. These distributions are computed from the barycentric flux data that have had the reactant energy spread removed by the deconvolution process. The widths of the angular distributions show a slight narrowing with increasing collision energy, consistent with decreased interaction times at higher kinetic energies. As the collision energy increases, the relative translational energy distributions of the products shift towards higher energies and increase in width. As a fraction of the total energy, the widths also increase, from 26% of the available energy at the lowest collision energy to 29% at the highest. The widths reflect the true values after deconvoluting the laboratory velocity distributions.

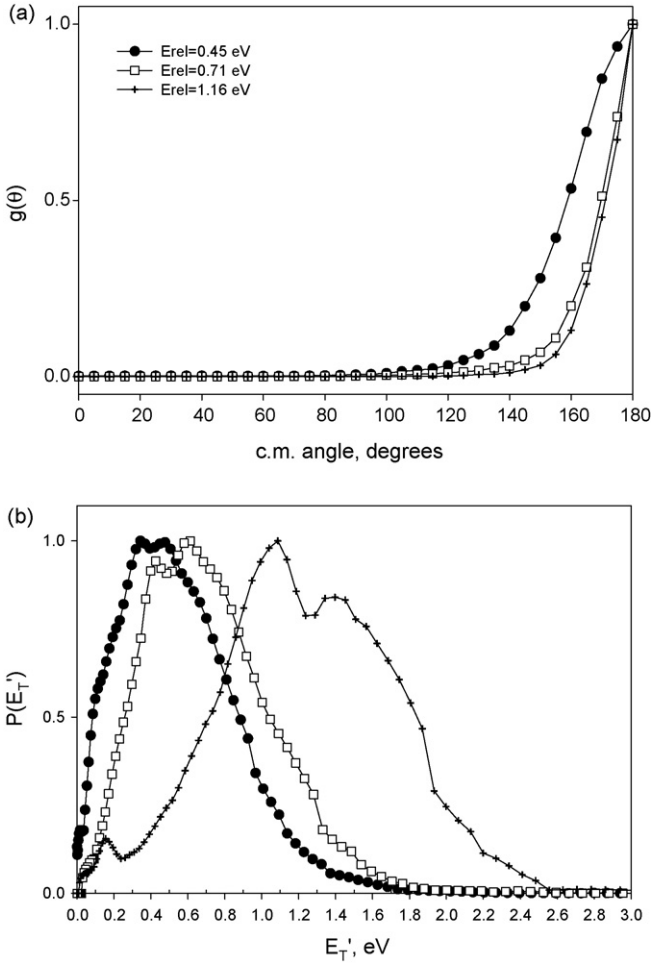

Fig. 2. (a) Angular distributions and (b) relative translational energy distributions for $C_3H_4^+$ products in c.m. coordinates at all energies.

Table 1
Energy results at different relative energies (in eV) for charge transfer reaction $OD^+ + C_3H_4 \rightarrow OD + C_3H_4^+$

Ion energy	0.61	0.98	1.64
Reactant relative energy, E_{rel}	0.45	0.71	1.16
Total energy, E_{total}	3.12	3.38	3.83
Product average relative energy, $\langle E'_T \rangle$	0.56	0.73	1.26
$\langle E'_T \rangle / E_{total}$ (%)	18.1	21.5	32.9
Product average internal energy	2.56	2.65	2.57
$Q = \langle E'_T \rangle - E_{rel}$	0.11	0.02	0.10

$\Delta H = -2.67$ eV.

The energy partitioning results for charge transfer are summarized in Table 1. The total energies of these collision systems are taken as the sums of the relative collision energy and the reaction exoergicity. The internal excitation of the C_3H_4 reactants, produced by supersonic expansion, is negligible. The vibrational excitation in the OD^+ reactants is more difficult to characterize. To the best of our knowledge, the internal energy distribution of OH^+ formed by dissociative ionization of H_2O [22] is not well-characterized. By analogy with the neutral system, where a translational spectroscopy study of the OH vibrational state distribution produced by 157 nm photolysis of H_2O shows that the population ratios of OH in $v = 0 : 1 : 2 : 3$ are approximately 1.0:1.1:0.60:0.30, respectively [23], we might expect a significant degree of nascent vibrational energy in the OD^+ reactants. However, neither this study nor our previous work [9–11] have indicated any thermochemical effects associated with reactant vibrational excitation. Thus, we neglect any reactant vibrational energy contribution to the total energy of the system. From energy conservation, we determine that the fraction of the total energy appearing in product translation increases from 18% to 33% as the collision energy spans the full range studied here. The average internal energy of the reaction products ranges from 2.56 to 2.65 eV at all collision energies, identical to the reaction exoergicity of 2.67 eV within 4%. Therefore, the internal energy distributions of the charge transfer products are essentially independent of collision energy in the range of these experiments.

The formation of mass 39 products may occur either by direct hydride transfer, process (2), or by dissociative charge transfer, process (5). Because the dissociation process is formally a unimolecular decay of excited $C_3H_4^+$, the $C_3H_3^+/C_3H_4^+$ ratio should increase markedly with collision energy if dissociative charge transfer makes a significant contribution to the $C_3H_3^+$ yield. In fact, this ratio remains constant over the 2.5-fold increase in collision energy of these experiments. This observation provides strong evidence against channel (5) as a significant route for $C_3H_3^+$ formation. We therefore conclude that $C_3H_3^+$ production occurs predominately via hydride transfer. The hydride transfer reaction was studied at collision energies of 0.50, 0.80 and 1.23 eV. Fig. 3 shows the flux distribution for the $C_3H_3^+$ products at the lowest collision energy. The major features of the distribution are both qualitatively and quantitatively similar to those for the charge transfer reaction, showing strong asymmetry with a maximum near the precursor propyne reactant velocity. The distributions for the two higher energy experiments are qualitatively similar to that shown in Fig. 3, and are included in Supplementary Information.

The product angular distributions and relative translational energy distributions at all three collision energies are shown in Fig. 4, with numerical results summarized in Table 2. The translational energy distributions are very similar to those of charge transfer products in that they broaden and shift with increasing collision energy. The results in Table 2 show that the average internal

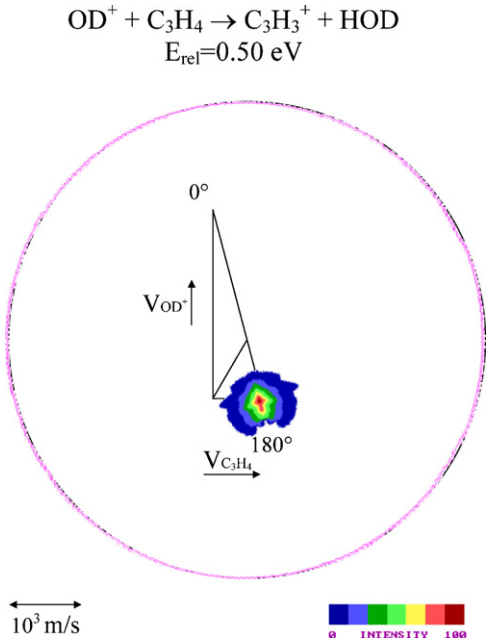

Fig. 3. Newton diagram and scattered $C_3H_3^+$ product flux contour map at the collision energy of 0.50 eV.

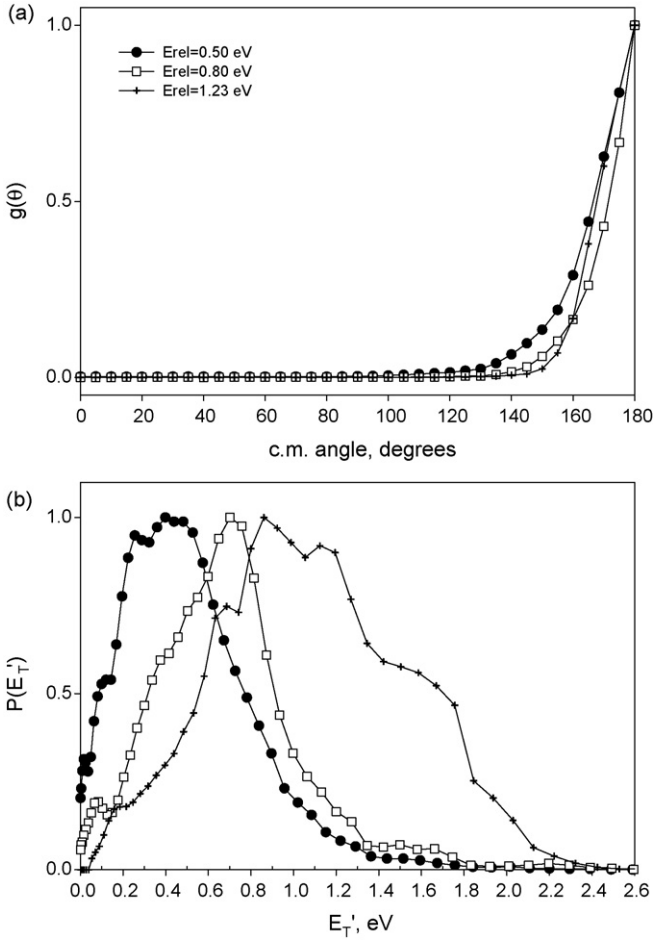

Fig. 4. (a) Angular distributions and (b) relative translational energy distributions for $C_3H_3^+$ product in c.m. coordinates at all energies.

Table 2
Energy results at different relative energies (in eV) for hydride transfer reaction $OD^+ + C_3H_4 \rightarrow HOD + C_3H_3^+$

Ion energy	0.67	1.12	1.74
Reactant relative energy, E_{rel}	0.50	0.80	1.23
Total energy, E_{total}	7.11	7.41	7.84
Product average relative energy, $\langle E'_T \rangle$	0.52	0.70	1.12
$\langle E'_T \rangle / E_{total}$ (%)	7.4	9.5	14.1
Product average internal energy	6.58	6.71	6.73
$Q = \langle E'_T \rangle - E_{rel}$	0.02	−0.10	−0.11

$\Delta H = -6.61$ eV.

energies of reaction products increase slightly as collision energy increased.

4. Computational results

In order to understand the role that possible reactive intermediates and the transition states connecting them play in the present system, we performed DFT calculations with the Gaussian 03 suite of programs [24]. The geometries of relevant species were fully optimized at the B3LYP/6-311+G* level of theory. Vibrational frequencies of intermediates and the transition states connecting them were extracted from the geometries in the harmonic approximation. Single point energy calculations based on geometries and zero-point vibrational energies were performed at the same level of theory. Benchmark computational studies [25] show that barriers for hydrogen atom transfer reactions at this level of theory are generally underestimated by as much as 30 kJ/mol, a point addressed in the appropriate discussion. Fig. 5 shows a schematic reaction coordinate incorporating these structures. Full details of the structures of reactants, products, intermediates, and transition states, including energies and vibrational frequencies, are reported in Supplementary Information for this article.

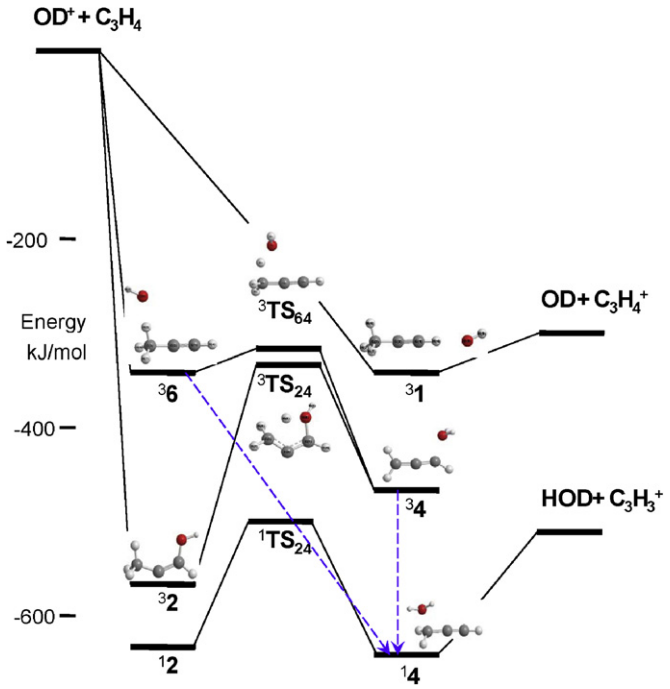

Fig. 5. Schematic reaction coordinate for $OD^+ + C_3H_4$ charge transfer and hydride transfer reactions. Major triplet state intermediates from DFT calculations as described in text are included. Dashed arrows denote possible intersystem crossing routes. All structures are reported in Supplementary Information for this article.

The OD^+ and C_3H_4 reactants are triplet and singlet state species respectively. The potential surface of approaching reactants has triplet multiplicity, and charge transfer products can form directly on this triplet surface. However, the products of hydride transfer, HOD and $C_3H_3^+$, are singlet state species. Therefore, the role of electron spin, particularly how intersystem crossing may play a critical role in governing the nature of the hydride transfer process, must be considered. Therefore, we have performed DFT calculations for surfaces of both singlet and triplet multiplicity.

The structures of possible intermediates for charge and hydride transfer were probed by first allowing the OH^+ reactant to approach the hydrogen atoms in propyne in turn. The interaction of OH^+ with the acetylenic hydrogen atom produced one intermediate, denoted ^{3}**1**, that corresponds to a triplet structure in which the reactants are electrostatically bound in a near-collinear configuration with a C—H···O—H motif. Electron density analysis indicates that the C_3H_4 moiety is charged, demonstrating that electron transfer has already occurred prior to the formation of the electrostatic complex. Complex ^{3}**1** is stable relative to reactants by 343 kJ/mol. Fig. 5 shows complex ^{3}**1** correlating directly with the charge transfer products.

The nominal $C_3H_3^+$ product of hydride abstraction may occur in four isomeric forms. The cyclopropenylium cation is lowest in energy, followed by the linear propargylium ion, $[CH_2C{\equiv}CH]^+$. The second of these species is the expected product of hydride abstraction from the methyl carbon of propyne. The barrier to interconversion between these two species is 356 kJ/mol relative to propargylium, in good agreement with earlier work by Liu [26]. Two other isomers, $[CH_2CH{=}C]^+$, structure **3** in Supplementary Information; and $[CH_3C{\equiv}C]^+$, are also possible products, the latter a result of hydride abstraction from the terminal acetylene carbon; our calculations produced a structure for this species at the HF/-31 G* level of theory, but further optimization at the B3LYP level failed to produce a stable structure. Our observation that hydride abstraction does not occur in the reaction of OD^+ with HC≡CH provides additional empirical evidence against abstraction of the acetylenic hydrogen in propyne.

Hydride transfer from C_3H_4 to OD^+ cannot occur in a single step, because ground state OD^+ does not have a low energy vacant orbital that can accept a pair of electrons, as required to form ground state HOD. In previous work from our laboratory [11], we have discussed two mechanisms whereby hydride transfer from an unsaturated hydrocarbon to OD^+ can occur. The discussion here will follow that previous work. In the hydride abstraction reaction of OD^+ with C_2H_4 [9], the experimental data were consistent with the formation of a triplet diradical oxirane cation $\dot{C}H_2CH_2\dot{O}D$ that underwent rapid internal conversion to the singlet manifold. In the ground singlet state, hydrogen migration and C—O bond cleavage led to product formation on a time scale comparable to a rotational period of the intermediate complex, evidenced by forward–backward asymmetry in the product angular distribution. In the reaction of OD^+ with propylene, hydride abstraction through the analogous oxirane did not appear to occur. The additional methyl group in the intermediate complex provided enough steric hindrance to create an entropic bottleneck along this pathway, allowing hydride abstraction via a sequential electron transfer/hydrogen atom transfer process to become more favorable.

DFT calculations to characterize the oxirene species formed by attack of OD^+ on the unsaturated carbons in propyne produced two complexes, denoted ^{3}**2** and ^{3}**3**, where the multiplicity of the complex is indicated explicitly. Complex ^{3}**2**, in which OD^+ attacks the terminal unsaturated carbon atom, lies 580 kJ/mol below the reactants, and is ~30 kJ/mol more stable than species ^{3}**3** formed by attack on the central carbon atom. Only the more stable species are shown in Fig. 5. Hydrogen atom migration from the methyl carbon to the oxygen atom over a 247 kJ/mol barrier transforms ^{3}**2** into complex ^{3}**4**. Rapid intersystem crossing of complex ^{3}**4** to its singlet analog, denoted ^{1}**4**, expected because of the favorable orientation of the orbitals containing the unpaired electrons [8,27], yields a suitable singlet precursor to products. The dashed line in Fig. 5 represents this process. We note that rapid intersystem crossing has been invoked to interpret the dynamics and product branching ratios of the isoelectronic $O(^3P)$ + propyne reaction [17].

The experimental data for $C_3H_3^+$ formation are consistent with a direct process that takes place on a time scale significantly shorter than the rotational period of any transient intermediate, on the order of 10^{-13} s. In order to assess which, if any, of the pathways revealed by the DFT calculations are relevant to the dynamics, we have computed rate constants according to Rice–Ramsperger–Kassel–Marcus (RRKM) theory [28], evaluating vibrational energy level sums and densities using frequencies extracted from the DFT calculations. Vibrational frequencies for all intermediates and transition states are tabulated in Supplementary Information. The rate constants are much more sensitive to the values of isomerization barrier energies than to precise values of vibrational frequencies; thus, the greatest systematic error in the rate calculations likely comes from the consistent underestimation of DFT-computed barrier heights [25]. The computed rate constants therefore represent upper limits. Nevertheless, the primary purpose of the rate constant calculations is to provide a qualitative assessment of the computed reaction paths that may have rates approaching the value of 10^{13} s^{-1} that one associates with a direct reaction.

The rate-limiting step for the oxirene pathway to products is the ^{3}**2** → ^{3}**4** isomerization step. The RRKM rate constant, using computed vibrational frequencies for complex ^{3}**2** and the transition state ^{3}**TS$_{24}$** for the isomerization process, is 4×10^9 s^{-1}, at least four orders of magnitude too slow to be compatible with the direct dynamics observed for this process. A similar analysis with complexes ^{3}**3** and ^{3}**5**, not explicitly shown in Fig. 5, in which the initial oxirene complex is formed by OD^+ attack on the central carbon, also shows that the rate-limiting step for product formation, $\sim 2 \times 10^9$ s^{-1}, is too slow to account for the experimental results.

We also considered the possibility that intersystem crossing in the initial oxirene may precede hydrogen migration. Using complex ^{3}**2** as an example, we found that the corresponding singlet species, ^{1}**2**, is 54 kJ/mol lower in energy. The singlet species ^{1}**4** lies 167 kJ/mol below the triplet species, and the transition state connecting them is 132 kJ/mol above ^{1}**2**. The RRKM rate constant for this isomerization is 9×10^{10} s^{-1}, also appearing to rule out this route for hydride transfer. A similar analysis for complexes ^{3}**3** and ^{3}**5** and their singlet counterparts produces a similar result. The conclusion from these calculations is that any pathway to hydride transfer involving an initial triplet oxirene species is much too slow to account for the experimental results that the process occurs on a time scale short compared to the rotational period of any intermediate complex. The structures of the complexes and transition states for this isomerization process are presented in Supplementary Information.

We also examined possible hydride abstraction pathways that proceeded through the interaction of the oxygen end of OD^+ with one of the hydrogen atoms bound to the methyl carbon. As indicated in Fig. 5, this approach geometry produces a triplet species, designated complex ^{3}**6**, where one of the hydrogen atoms bound to the methyl carbon has moved toward the approaching OD^+. Analysis of the charge on this species indicates that electron transfer from C_3H_4 to OD^+ has occurred, and is therefore a triplet OD—$C_3H_4^+$ adduct.

Migration of one of the methyl hydrogens toward the oxygen atom in complex ^{3}**6** was found to proceed through a transition state denoted ^{3}**TS$_{64}$**, which ultimately evolved to complex ^{3}**4**. Subsequent rapid intersystem crossing to the ^{1}**4** complex would lead to

ground state products, with the $^3\mathbf{6} \rightarrow {}^3\mathbf{4}$ barrier limiting the rate of hydride transfer. The calculations showed that $^3\mathbf{TS_{64}}$ lies 26 kJ/mol above $^3\mathbf{6}$, yielding a $^3\mathbf{6} \rightarrow {}^3\mathbf{4}$ isomerization rate of $\sim 6 \times 10^{11}$ s^{-1}, the fastest among the isomerization rates we have found on these surfaces, but still too slow to account for the strongly asymmetric angular distribution for hydride transfer.

As discussed in our previous work [11], intersystem crossing in the initially formed $^3\mathbf{6}$ adduct should be rapid, because of the fact that in the electrostatically bound OD—$C_3H_4^+$ complex, the orbitals in which the unpaired electrons reside can achieve a perpendicular configuration where spin–orbit matrix elements are non-zero [27]. However, a recent discussion of intersystem crossing in the $O^+ + C_2H_2$ system [29] suggested that the process is slow but can be facilitated by bending vibrations in C_2H_2. A detailed study of this process in the OD—$C_3H_4^+$ system could help clarify the issue. The DFT calculations failed to produce a stable singlet analog of complex **6**, resulting instead in the collapse of all singlet structures to the optimized configuration of complex $^1\mathbf{4}$, in which hydrogen atom transfer has already occurred. This complex undergoes simple bond cleavage through a loose transition state. The decay rate for complex $^1\mathbf{4}$ to products is in excess of 10^{13} s^{-1}, comparable in magnitude to the rate of intersystem crossing. Thus, the rate-limiting step is faster than the rotational period of the transient association complex of approaching reactants, producing the asymmetric angular distribution of products observed in this study. The data are therefore inconsistent with initial formation of an oxirane diradical cation, but consistent with a sequential charge transfer-hydrogen atom transfer process.

Fig. 5 summarizes the major reaction pathways for charge and hydride transfer. All structures are reported in the online Supplementary Information.

5. Discussion

The dynamics of the hydride transfer process appear to be direct. Interestingly, the average values of the product kinetic energy are reasonably consistent with the predictions of the impulsive Spectator Stripping (SS) model proposed over 40 years ago [30] to describe hydrogen atom transfer reactions in $X^+ + H_2$ collisions. In the present experiment, where the collision energy is at most 25% of the energies of the bonds being broken and formed, an impulsive model that treats particles as hard spheres would not be expected to be valid. The agreement with this simple model is fortuitous, largely because the final velocity of $C_3H_3^+$ is tightly constrained by momentum conservation to lie very close to that of the reactant C_3H_4, irrespective of dynamics. Even more important, the SS model completely ignores any details of electronic structure, particularly the critical role of electron spin in directing the formation of products. The preceding discussion of the nature of reactive intermediates and the transition states separating them makes the point that one must address the structures of important triplet and singlet intermediates to understand hydride transfer.

The asymmetric angular distribution observed for the propyne system allows us to reject reactive pathways in which the OD^+ reactant adds to the C≡C bond to form a triplet state diradical oxirane cation. Instead, the calculations support the mechanism we have proposed in previous work [11], in which collisions of OD^+ with the methyl hydrogens result in an initial long range charge transfer process. Intersystem crossing in the triplet state adduct yields structures in which hydrogen atom transfer occurs spontaneously.

Reactive collisions also provide additional insight into features of the potential surface topology beyond the regions where intersystem crossing is probable. Hydride transfer often exhibits energy disposal motifs that are kinematically determined. Hydride transfer, like proton and hydrogen atom transfer, is an example of a heavy + light-heavy (H + LH) system in which a light particle, hydrogen in this case, is transferred between heavier molecular fragments. The coordinates that diagonalize the quadratic form for the kinetic energy [31] are scaled and skewed in a manner that depends on the mass of the particle transferred, M_L, and the masses of the heavy groups donating and accepting the transferred particle, denoted M_1 and M_2, respectively. The skewing angle β, the angle that the exit channel valley makes with respect to the entrance valley, is calculated from the expression $\tan\beta = M_L M_{total}/(M_1 M_2)$, and equals 16° for the particular mass combination for this experiment. Such an acute angle between the entrance and exit channels for light particle transfer has a significant effect on reactive trajectories and energy disposal in such reactions. At low collision energy, reactive trajectories may not have sufficient energy to penetrate into the corner of such highly skewed surfaces, where the forming and breaking bonds are both compressed. Instead, trajectories will have a strong propensity to cut the corner separating the entrance and exit valleys. This motion corresponds to light atom transfer from a configuration in which both the cleaving and incipient bonds are extended from equilibrium. Under these conditions, the nascent bond is formed in an extended configuration, yielding reaction products that are vibrationally excited. This mechanism is described as "mixed energy release" [32–35]. The hydride transfer data reported here at the lowest collision energy show that 93% of the available energy is partitioned in product internal excitation. Almost the entire reaction exoergicity is transformed into internal excitation, consistent with an early release of the exoergicity, as expected for mixed energy release.

More detailed insight into the reactive dynamics comes from the experimental data at higher collision energies. The increase in reactant translational energy between experiments performed at successive collision energies is called the "incremental" translational energy. The concept of "induced repulsive energy release" was introduced to address partitioning of the incremental translational energy on H + LH potential surfaces [36], focusing on the fact that the incremental energy allows the reactive system to probe a qualitatively different, and generally repulsive, region of the potential energy surface relative to the baseline energy. In this picture, reactive trajectories with excess translation penetrate far into the corner of the highly skewed potential surface where both the forming and breaking bonds are compressed. The trajectory moves into the exit valley with little motion perpendicular to the reaction coordinate, yielding products with high translational excitation. As the collision energy increases from 0.50 to 0.80 eV, Table 2 shows that the average kinetic energy of the products increases from 0.52 to 0.70 eV. Thus, at 0.80 eV, 60% of the incremental translational energy appears in product translation. Similarly, at the highest collision energy of 1.23 eV, a significantly increased fraction, 94% of the incremental translational energy, partitions into product translation. The corner cutting trajectories that produce vibrationally excited products at lower collision energies are replaced by trajectories at higher translational energy that are significantly more effective at reaching the compressed configurations that facilitate translation in the separating products. This hydride transfer reaction provides an excellent example of "induced repulsive energy release".

The charge transfer process observed here, which appears to proceed as a direct reaction with a long-range electron jump, is also worthy of additional comment. Table 1 shows that values of the translational exoergicity Q, defined as the difference between the relative kinetic energies of products and reactants, at all three collision energies, are very close to zero, indicating near-resonance between the kinetic energies of the reactants and products. Since the neutral product is formed along the same direction as the incoming ion, this result also implies that there is almost

no momentum transfer accompanying charge transfer, a conclusion consistent with collisions that occur through large impact parameters.

Although ion–neutral collisions are often influenced by motion over a substantial portion of the operative potential surface or surfaces, it has been established in many cases that electron-transfer reactions at thermal energies are subject to energy resonance and Franck-Condon effects [37,38]. In the present system, the recombination energy of OH^+ is 13.02 eV [39]. There is no matching band at this energy in the photoelectron spectrum of C_3H_4. The closest ionic state is at 14.70 eV [40]. Similarly, the $\mathbf{A}^2\Sigma^+$ state of OH lies 4.05 eV above the ground state [41], significantly above the 2.67 eV exoergicity of the charge transfer process. Although vibrationally excited OD^+ reactants could more closely satisfy the energy resonance condition, earlier discussion suggests that this level of vibrational excitation is not likely found with significant population.

Therefore neither energy resonance nor favorable Franck-Condon factors are operative in guiding the charge transfer process. As discussed by Mayhew [42], distortion of the molecular potential surface by the electric field of the reacting ion, leading to a significant changes in the Franck-Condon factors prior to charge transfer, may account for the observation of efficient charge transfer reactions involving polyatomic species with large polarizability, where the recombination energy of the ion falls outside the Franck-Condon envelope of a photoelectron band. Previous results from this laboratory on the $OD^+ + C_2H_2$ system appear to be consistent with this principle [10]. The larger polarizability of C_3H_4, $\sim 5.3 \times 10^{-24}$ cm^3 [43], suggests that such distortions are even more likely to play a significant role in the present case, providing some rationalization for the energy distributions in the products.

6. Conclusions

The crossed beam technique and DFT calculations have been used to study the reaction dynamics of charge transfer and hydride transfer between OD^+ and C_3H_4. The product c.m. flux distributions of both reactions at three energies exhibit sharp asymmetry, with the maxima close to the velocity and direction of the precursor propyne beam. The results indicate that both reactions occur on a time scale significantly less than the rotational period of the transient intermediate formed by the approaching reactants. The charge transfer reaction places a constant amount of energy in the products, suggesting that the electron is transferred at long distances, before the approaching reactants exert a significant attraction on one another. Despite the lack of energy resonance and favorable Franck-Condon factors, a distortion in the Franck-Condon envelope of C_3H_4 may contribute to the efficiency of the charge transfer reaction.

The absence of a low energy vacant orbital on OD^+ to accept an electron pair during the formation of ground state HOD requires that hydride transfer involve a change in multiplicity during the reaction. DFT calculations have provided evidence against pathways in which the OD^+ attacks an unsaturated carbon atom to form a diradical that undergoes rapid intersystem crossing to the singlet manifold with subsequent hydrogen atom transfer. Isomerization rates on the ground state surface calculated with RRKM theory are too slow to be compatible with the direct dynamics observed. Instead, a mechanism based on initial charge transfer to form an $OD{-}C_3H_4^+$ adduct, followed by efficient intersystem crossing and rapid hydrogen atom, appears to be consistent with the experimental data. The kinematics associated with the H + LH mass combination also come into play in this reaction. The reaction shows characteristics of both mixed energy release and induced repulsive energy release as a consequence of the small skew angle between the entrance and exit valleys.

The $OD^+ + C_3H_4$ reaction demonstrates the value of quantum chemical structural calculations in interpreting the results of crossed beam experiments. We expect the synergy between experiment and theory to strengthen, as next-generation methods in both areas of inquiry experience new and exciting developments.

Acknowledgements

The authors wish to express their gratitude to Professor Zdenek Herman for the leadership and vision that he has given to the field of ion–neutral interactions throughout his long and productive scientific career. J.M.F. is especially appreciative of Professor Herman's support, encouragement, and friendship. We are grateful to the University of Rochester for fellowship support of this research. We also appreciate helpful conversations with Professor Joseph P. Dinnocenzo.

Appendix A. Supplementary data

Supplementary data associated with this article can be found, in the online version, at doi:10.1016/j.ijms.2008.08.002.

References

[1] R. Cvetanovic, Adv. Photochem. 1 (1963) 115.
[2] P. Casavecchia, G. Capozza, E. Segoloni, F. Leonori, N. Balucani, G.G. Volpi, J. Phys. Chem. A 109 (2005) 3527.
[3] T.L. Nguyen, L. Vereecken, X.J. Hou, M.T. Nguyen, J. Peeters, J. Phys. Chem. A 109 (2005) 7489.
[4] I.W.M. Smith, Chem. Soc. Rev. 37 (2008) 812.
[5] G.D. DeBoer, J.A. Dodd, J. Phys. Chem. A 111 (2007) 12977.
[6] L.K. Huynh, S.W. Zhang, T.N. Truong, Combust. Flame 152 (2008) 177.
[7] M. Dupuis, J.J. Wendolowski, T. Takada, W.A. Lester Jr., J. Chem. Phys. 76 (1982) 481.
[8] K. Yamaguchi, S. Yabushita, T. Fueno, S. Kato, K. Morokuma, Chem. Phys. Lett. 80 (1980) 27.
[9] X. Cai, Y. Li, J.M. Farrar, Int. J. Mass Spectrom. 241 (2005) 271.
[10] L. Liu, C. Martin, J.M. Farrar, J. Chem. Phys. 125 (2006) 133117.
[11] L. Liu, E.S. Richards, J.M. Farrar, J. Chem. Phys. 127 (2007) 244315.
[12] G. Bouchoux, J.P. Flament, Y. Hoppilliard, Nouveau Journal de Chimie 7 (1983) 385.
[13] J.R. Kanofsky, D. Lucas, F. Pruss, D. Gutman, J. Phys. Chem. 78 (1974) 311.
[14] B. Blumenberg, K. Hoyermann, R. Sievert, Symp. (Int.) Combust. [Proc.] 16 (1976) 841.
[15] C.A. Arrington, D.J. Cox, J. Phys. Chem. 79 (1975) 2584.
[16] M.E. Umstead, R.G. Shortridge, M.C. Lin, Chem. Phys. 20 (1977) 271.
[17] G. Xing, X. Huang, X. Wang, R. Bersohn, J. Chem. Phys. 105 (1996) 488.
[18] D.F. Varley, D.J. Levandier, J.M. Farrar, J. Chem. Phys. 96 (1992) 8806.
[19] Z. Herman, Int. J. Mass Spectrom. 212 (2001) 413.
[20] M.L. Vestal, C.R. Blakley, J.H. Futrell, Phys. Rev. A 17 (1978) 1321.
[21] P.E. Siska, J. Chem. Phys. 59 (1973) 6052.
[22] J.D. Morrison, J.C. Traeger, Int. J. Mass Spectrom. Ion Phys. 11 (1973) 77.
[23] D.W. Hwang, X.F. Yang, X.M. Yang, J. Chem. Phys. 110 (1999) 4119.
[24] M.J. Frisch, G.W. Trucks, H.B. Schlegel, G.E. Scuseria, M.A. Robb, J.R. Cheeseman, J.A. Montgomery Jr., T. Vreven, K.N. Kudin, J.C. Burant, J.M. Millam, S.S. Iyengar, J. Tomasi, V. Barone, B. Mennucci, M. Cossi, G. Scalmani, N. Rega, G.A. Petersson, H. Nakatsuji, M. Hada, M. Ehara, K. Toyota, R. Fukuda, J. Hasegawa, M. Ishida, T. Nakajima, Y. Honda, O. Kitao, H. Nakai, M. Klene, X. Li, J.E. Knox, H.P. Hratchian, J.B. Cross, C. Adamo, J. Jaramillo, R. Gomperts, R.E. Stratmann, O. Yazyev, A.J. Austin, R. Cammi, C. Pomelli, J.W. Ochterski, P.Y. Ayala, K. Morokuma, G.A. Voth, P. Salvador, J.J. Dannenberg, V.G. Zakrzewski, S. Dapprich, A.D. Daniels, M.C. Strain, O. Farkas, D.K. Malick, A.D. Rabuck, K. Raghavachari, J.B. Foresman, J.V. Ortiz, Q. Cui, A.G. Baboul, S. Clifford, J. Cioslowski, B.B. Stefanov, G. Liu, A. Liashenko, P. Piskorz, I. Komaromi, R.L. Martin, D.J. Fox, T. Keith, M.A. Al-Laham, C.Y. Peng, A. Nanayakkara, M. Challacombe, P.M.W. Gill, B. Johnson, W. Chen, M.W. Wong, C. Gonzalez, J.A. Pople, Gaussian 03, Gaussian, Inc., Wallingford, CT, 2004.
[25] J. Zheng, Y.J. Zhao, D.G. Truhlar, J. Chem. Theory Comput. 3 (2007) 569.
[26] G.-x. Liu, Z.-s. Li, Y.-h. Ding, Q. Fu, X.-R. Huang, C.-C. Sun, A.C. Tang, J. Phys. Chem. A 106 (2002) 10415.
[27] L. Salem, C. Rowland, Angew. Chem. Int. Ed. 11 (1972) 92.
[28] R.A. Marcus, J. Chem. Phys. 20 (1952) 359.
[29] K. Fukuzawa, T. Matsushita, K. Morokuma, D.J. Levandier, Y.H. Chiu, R.A. Dressler, E. Murad, A. Midey, S. Williams, A.A. Viggiano, J. Chem. Phys. 115 (2001) 3184.

[30] A. Henglein, K. Lacmann, G. Jacobs, Ber. Bunsenges. Phys. Chem. 69 (1965) 279.
[31] J.O. Hirschfelder, Int. J. Quantum Chem. Symp. 3 (1969) 17.
[32] K.G. Anlauf, P.J. Kuntz, D.H. Maylotte, P.D. Pacey, J.C. Polanyi, Discuss. Faraday Soc. 44 (1967) 183.
[33] K.G. Anlauf, J.C. Polanyi, W.H. Wong, K.B. Woodall, J. Chem. Phys. 49 (1968) 5189.
[34] D.H. Maylotte, J.C. Polanyi, K.B. Woodall, J. Chem. Phys. 57 (1972) 1547.
[35] C.A. Parr, J.C. Polanyi, W.H. Wong, J. Chem. Phys. 58 (1973) 5.
[36] A.M.G. Ding, L.J. Kirsch, D.S. Perry, J.C. Polanyi, J.L. Schreiber, Faraday Disc. Chem. Soc. 55 (1973) 252.
[37] M.T. Bowers, D.D. Elleman, Chem. Phys. Lett. 16 (1972) 486.
[38] J.B. Laudenslager, W.T. Huntress, M.T. Bowers, J. Chem. Phys. 61 (1974) 4600.
[39] NIST, http://webbook.nist.gov/chemistry/, 2005.
[40] K. Kimura, S. Katsumata, Y. Achiba, T. Yamazaki, S. Iwata, Handbook of HeI Photoelectron Spectra of Fundamental Organic Molecules, Halsted Press, New York, 1980.
[41] K.P. Huber, G. Herzberg, Constants of Diatomic Molecules, Van Nostrand, New York, 1979.
[42] C.A. Mayhew, J. Phys. B: At. Mol. Opt. Phys. 25 (1992) 1865.
[43] G.H. Ho, M.S. Lin, Y.L. Wang, T.W. Chang, J. Chem. Phys. 109 (1998) 5868.